January 22, 2003

Emergence of multiple Fermi surface maps in angle-resolved photoemission from $Bi_2Sr_2CaCu_2O_8+\delta$

M. C. Asensio
Instituto de Ciencias de Materiales de Madrid

J. Avila
Instituto de Ciencias de Materiales de Madrid

L. Roca
Instituto de Ciencias de Materiales de Madrid

A. Tejeda
Instituto de Ciencias de Materiales de Madrid

G. D. Gu
Brookhaven National Laboratory

See next page for additional authors

Emergence of multiple Fermi surface maps in angle-resolved photoemission from $Bi_2Sr_2CaCu_2O_{8+\delta}$

M. C. Asensio,[1,2,*] J. Avila,[1,2] L. Roca,[1,2] A. Tejeda,[1,2] G. D. Gu,[3] M. Lindroos,[4,5] R. S. Markiewicz,[5] and A. Bansil[5]
[1]*Instituto de Ciencias de Materiales de Madrid (CSIC), 28049 Cantoblanco, Madrid, Spain*
[2]*LURE, Bât. 209D, Université Paris-Sud, BP34, 91898 Orsay, France*
[3]*Physics Department, Building 510B, Brookhaven National Laboratory, Upton, New York 11975-5000*
[4]*Institute of Physics, Tampere University of Technology, 33101 Tampere, Finland*
[5]*Department of Physics, Northeastern University, Boston, Massachusetts 02115*
(Received 19 September 2002; published 22 January 2003)

We report angle-resolved photoemission spectra (ARPES) for emission from the Fermi energy (E_F) over a large area of the (k_x,k_y) plane using 21.2 and 32 eV photon energies in two distinct polarizations from an optimally doped single crystal of $Bi_2Sr_2CaCu_2O_{8+\delta}$ (Bi2212), together with extensive first-principles simulations of the ARPES intensities. The results display a wide-ranging level of accord between theory and experiment, demonstrating that the ARPES matrix elements can produce a striking variety of Fermi surface maps, especially in the presence of secondary features arising from modulations of the underlying tetragonal system. Our analysis demonstrates how the energy and polarization dependency of the ARPES matrix element can help to disentangle the primary contributions to the spectrum from the secondary features and indicates that secondary features reflect a direct modulation of the CuO_2 planes.

DOI: 10.1103/PhysRevB.67.014519 PACS number(s): 74.72.−h, 71.18.+y

I. INTRODUCTION

Angle-resolved photoemission has undergone a revolution in the last few years as great strides have been taken in energy and momentum resolution. Particularly in connection with the high-T_c superconducting compounds, these advances portend fundamental progress in understanding the nature of strong coupling effects, including Mott gaps, spin-charge separation, pseudogap and stripes, so that a robust picture of the normal and the superconducting state of these materials can be adduced. $Bi_2Sr_2CaCu_2O_{8+\delta}$ (Bi2212) has played an essential role in much of this work, although ARPES studies of other high-T_c's are increasingly becoming feasible as techniques for obtaining high quality single crystal surfaces have improved.[1]

Progress on these problems has been contributed by various ARPES groups. A few highlights pertinent to the present work are as follows. On the specific issue of the number and type of FS sheets, beautiful recent work has been reported on Bi2212, Bi2201, and Pb-substituted Bi2212.[2–9] The importance of modulations in analyzing the ARPES data on Bi2212, especially of the ''shadow'' features[10] arising from the orthorhombic modulation, and the ''Umklapp replicas'' from the superlattice modulation has been emphasized early by Refs. 11,12. References 13,14 have concentrated on the role of stripes. The value of considering momentum distribution curves (rather than the traditional energy distribution curves) in the ARPES spectra has been pointed out by Ref. 15.

A complication in interpreting ARPES spectra of Bi2212 taken over a large area of the (k_x,k_y) plane is that different groups report an apparent multiplicity of strikingly different FS maps obtained for emission from the Fermi energy. Here we demonstrate that much of this variability is inherent and arises from the character of photoemission matrix element and its dependence on photon energy and polarization. Comparison of extensive first-principles simulations with experiments on a single sample reveals a remarkable, wide-ranging level of agreement between experiment and theory, with individual maps dominated by matrix elements and modulations due to secondary ''shadow'' and ''Umklapp'' features, despite the presence of a single underlying bulk electronic structure. Our analysis indicates that the secondary features possess a matrix element which is intrinsically different from that for the primary features. By a proper choice of photon energy and polarization specific features in the underlying electronic spectrum can thus be highlighted in general, and in particular, closely placed Fermi sheets can be disentangled; our data confirms the existence of two FS sheets at optimal doping.[2,3,5,7]

II. EXPERIMENTAL DETAILS

High quality single crystals of optimally doped Bi2212 (T_c=90 K) were grown by the traveling solvent floating zone method with an infrared mirror furnace. The very good long range order and low defect density is indicated by the narrow transition width of 1 K (measured by SQUID), and by x-ray diffraction rocking curve measurements. The FS maps were produced by measuring the photointensity within a narrow energy window at E_F over the full 360° angular range in the (k_x,k_y) plane at the SU8 high-resolution beamline of the Super-Aco synchrotron ring at LURE.[16,17] The data were collected on a regular mesh in polar (θ) and azimuthal angles (ϕ) of steps $\Delta\theta=1^o$, $\Delta\phi=1^o$. The PGM monochromator is equipped with six gratings to cover an energy range from 16 eV to 960 eV, with an average resolving power of 3×10^4 at 10^{11} photons/s. Some measurements employed He-I light (unpolarized) from a He discharge lamp. The overall energy resolution varied from 12 to 60 meV depending on measurement conditions.[18,19] The chamber base pressure was better than 5×10^{-11} mbar during the experiments. Procedure to assure an accurate sample align-

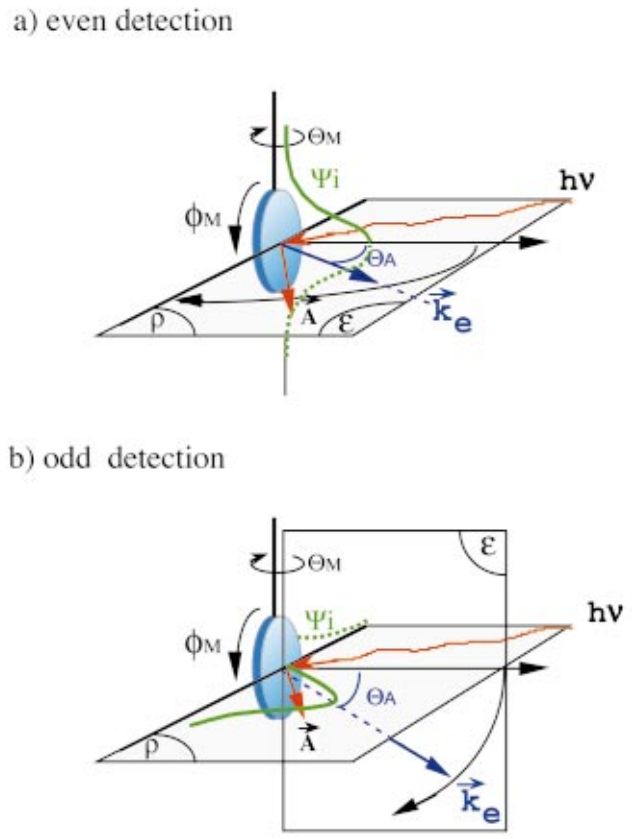

FIG. 1. (Color) The meaning of ''even'' and ''odd'' detection geometry in the present ARPES experiments is explained. $\vec{k}_e$ points toward the detector. In the even case, the detector moves in the plane of incident light (horizontal plane) in which the synchrotron light is polarized. In the odd case, the detector moves in a perpendicular plane as shown. The sample is kept fixed. For initial states lying in a mirror plane (e.g., along the $\bar{\Gamma}$-$\bar{M}$ line), the even polarization selects emission only from states symmetric with respect to the mirror plane, while the odd polarization couples to antisymmetric states as discussed in the text. The detector is rotated along the vertical and horizontal axis to access states throughout the (k_x,k_y) plane.

ment included a complete set of photoelectron diffraction azimuthal and polar scans of the Bi core level in the high-energy regime which were recorded *in situ* in order to define the $\bar{\Gamma}$ point and the main high symmetry directions.[20–22] For presentation purposes, a small background was subtracted from the experimental data, but all the features discussed below are also visible without this subtraction. The data have not been symmetry averaged.

Two different detection geometries—referred to as ''even'' and ''odd''—have been employed to obtain the ARPES spectra. In these measurements, the sample position is fixed, while the detector moves. As depicted in Fig. 1, in the even case, the detector is constrained to move in the horizontal plane, which is the *same* as the plane of the incident light, whereas for the odd case, the detector is chosen to move in the vertical plane. FS maps are constructed with the polarization always even (or odd) with respect to all the mirror planes, by rotating the detector so as to keep the incident light vector polarized along the radial (or tangential) direction with respect to the zone center $\bar{\Gamma}$ at every point in the (k_x,k_y) plane. It can then be shown that when emission from a mirror plane in the crystal lattice is involved (e.g., along the Γ-M line), the even (or odd) experiment only probes initial states of even (or odd) symmetry. To see this, observe first that in the case of a mirror plane the final state $|\Psi_f\rangle$ must be even in order to be observable—the odd state possesses a zero amplitude as the sketch in Fig. 1 shows. The dipole matrix element $\langle\Psi_f|\vec{p}\cdot\vec{A}|\Psi_i\rangle$, where $\vec{p}$ is the momentum operator, is then nonvanishing only for an even (or odd) initial state $|\Psi_i\rangle$ if the polarization (along the vector potential $\vec{A}$) is parallel (or perpendicular) to the mirror plane as is the case in the even (or odd) detection mode. At a general $k_\parallel$ point, even and odd measurements still provide some discrimination with respect to the character of the initial states. In the case of emission from the Cu-O planes in Bi2212, the relevant initial states are predominantly Cu $3d_{x^2-y^2}$ hybridized with O $2p_{x,y}$, and the band crossing E_F is antibonding, so that states along the $\bar{\Gamma}\rightarrow\bar{M}$ line (along the Cu-O-Cu bonds) will be intense in the even experiment, while states along $\bar{\Gamma}\rightarrow\bar{X}(\bar{Y})$ will be strong in the odd measurements.

III. COMPUTATIONAL DETAILS

All computations in this article are based on the one-step model of photoemission extended to treat arbitrarily complex unit cell materials.[23–28] Effects of multiple scattering and the ARPES matrix element[23] are thus included realistically in the presence of a specific surface termination, taken here to be the Bi-O layer. The finite lifetimes of the initial and final states are incorporated by giving suitable imaginary parts to the self-energies of the associated initial and final state propagators. The crystal potential was obtained via a self-consistent KKR procedure[29–31] assuming a perfect tetragonal lattice which yielded the well-known LDA-based band structure and FS of Bi2212.[32] The actual potential used in this work, however, has been modified slightly such that the Bi-O pockets around the $\bar{M}$ point are lifted above E_F to account for their absence in the experimental ARPES spectra. A number of simulations have also been carried out where repulsive barriers were placed between the two CuO_2 planes in the Ca layers in order to mimic correlation effects beyond the LDA which are expected to reduce the bilayer splitting. Finally, in order to describe the effects of the orthorhombic modulation and the $\sim(1\times5)$ superstructure present in Bi2212, we have taken the spectrum computed for the tetragonal case and superposed on this the same spectrum with appropriate weights after suitable translations in the reciprocal space. The weights used are estimated from relative intensities in the experimental FS maps and are summarized in Table I. The procedure for estimating the weights is described in the Appendix.

IV. RESULTS AND DISCUSSION

Figure 2 considers two sets of theoretical spectra at 21.2 eV in the even and odd detection geometries for the tetrag-

TABLE I. Relative fractional weights of various secondary features in Bi2212 obtained by analyzing the experimental FS maps where the primary spectrum for the tetragonal lattice is normalized to unity; see Appendix for details. The superlattice modulation gives the first and second Umklapp images, while the orthorhombic modulation yields the shadow feature and the related Umklapps. The translation vectors involved are of form $\eta(\pi,\pi)$ parallel to the orthorhombic b^* axis. Listed values of η come in pairs. First and second Umklapps roughly correspond to η values of $\pm 1/5$ and $\pm 2/5$, respectively.

$h\nu$	Detection geometry	Orthorhombic modulation		Superlattice modulation	
		shadows	1st Umklapps	1st Umklapps	2nd Umklapps
21.2 eV	even	0.10	0.01	0.20	0.01
	odd	0.30	0.15	0.40	0.02
32 eV	even	0.15	0.05	0.35	0.12
	odd	0.40	0.12	0.40	0.01
η [Translation vector is $\eta(\pi,\pi)$]		± 0.5	$+(0.5\pm 0.21)$ $-(0.5\pm 0.21)$	± 0.21	± 0.42

onal lattice, and helps set the stage for our discussion. The right hand Figs. 2(b), 2(d) refer to simulations where the bilayer splitting has been artificially reduced to a near zero value and both FS sheets are holelike around the $\bar{X}(\bar{Y})$ symmetry point. The case with a bilayer splitting of ~ 200 meV where the first FS sheet is holelike and the second sheet is slightly electronlike is depicted in the left hand Figs. 2(a), 2(c). We see by comparing Figs. 2(a) and 2(b) that there is a striking increase in the intensity around the $\bar{M}$ point for even detection due to the presence of the aforementioned second underlying FS sheet. By varying the size of the bilayer splitting and/or the position of E_F we have determined that this second band must be within $\sim \pm 20$ meV of E_F around the $\bar{M}$ point to produce such a large intensity feature. These results clearly show that matrix element effects can act to enhance or mask the ARPES signal from individual bands. This is a crucially important observation which we will recall below in analyzing the experimental data. Figure 2 also highlights the differences between the even and odd maps more generally. The second FS sheet so prominent in the even map of Fig. 2(a) is essentially ''invisible'' in the corresponding odd map of Fig. 2(c). Also, the odd map is complementary to the even map in the sense that regions of high intensity in one map are often replaced by those of low intensity in the other and vice versa; for example, in the even case, the intensity is low along the diagonal $\bar{\Gamma}\rightarrow\bar{X}(\bar{Y})$ lines, while in the odd case there is an intensity maximum along the diagonal associated with the hole sheets.

Figures 3 and 4 compare experimental and theoretical spectra at 21.2 and 32 eV, respectively. While changes in the ARPES maps of the FS with photon energy and polarization are striking, an excellent overall agreement with theory is seen in all cases. The unpolarized (He I) data [Fig. 3(a)] and theory [Fig. 3(b)] both show a clear imprint of the large hole sheet centered around $\bar{X}$ or $\bar{Y}$, but relatively little trace of the second FS sheet around $\bar{M}$. However, under even polarized light [Figs. 3(c), 3(d)] this second sheet comes alive giving intense emission around the $\bar{M}$ points. As emphasized already in connection with Fig. 2 above, the appearance of this large intensity is an unmistakable signature of the presence of a second band lying close to E_F at $\bar{M}$. Notably, secondary

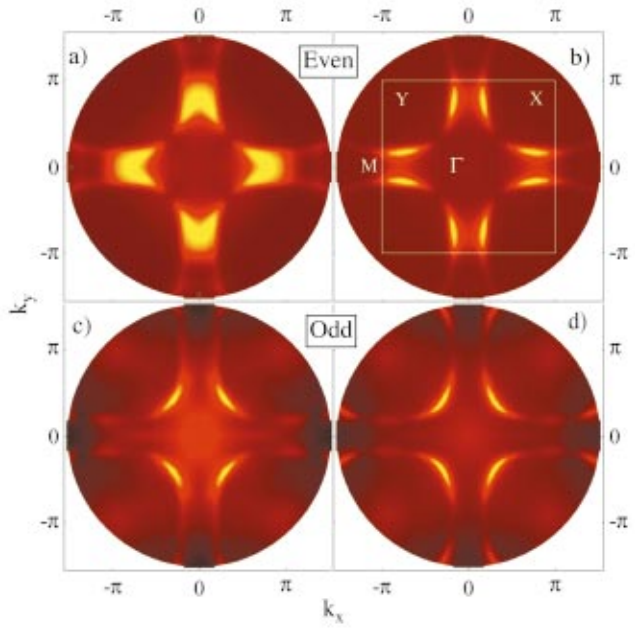

FIG. 2. (Color) Theoretical maps at 21.2 eV for emission from E_F in tetragonal Bi2212 for even and odd polarizations of light described in the text. The left hand simulations (a), (c) refer to the band theory-based crystal potential with a bilayer splitting of ~ 200 meV at the $\bar{M}$ point. In the right hand side simulations (b), (d), the bilayer splitting has been artificially reduced to a nearly zero value. Intensities are normalized to the same value in all maps and plotted in hot colors (whites and yellows are highs) on a linear scale. The square in solid white lines marks the 2D Brillouin zone.

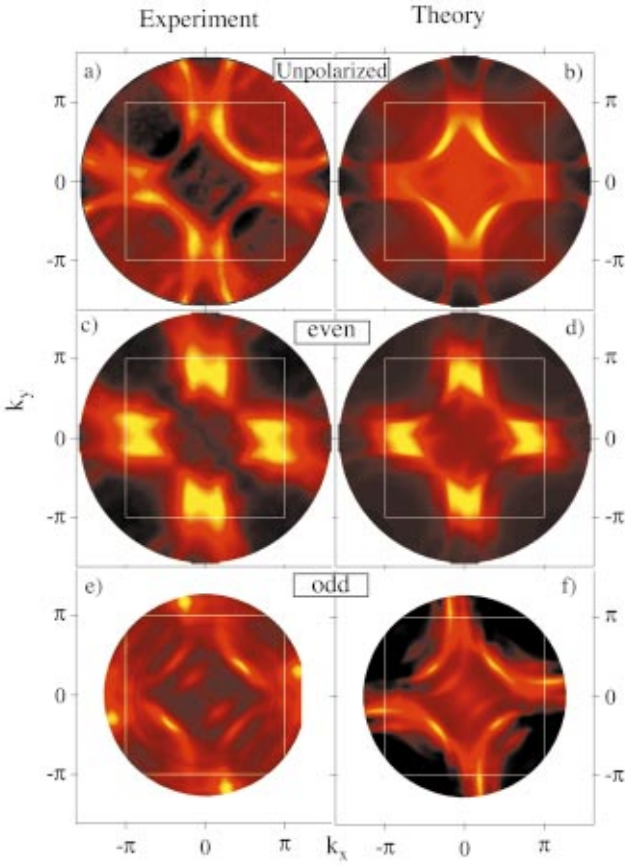

FIG. 3. (Color) Theory and experiment are compared directly at 21.2 eV for even and odd polarizations, as well as for the unpolarized He I light. Effects of superlattice and orthorhombic modulations are included in theory as discussed in the text. See caption to Fig. 2 for other pertinent details.

features are quite weak under these experimental conditions (21.2 eV, even—Table I, below) and, therefore, can be essentially ignored in the analysis of Figs. 3(c), 3(d). Detailed modeling leads us to conclude that within the present experimental resolution we cannot determine the position of this band with respect to the Fermi level better than ± 20 meV, and hence cannot say whether it is slightly electronlike or holelike.

Under odd polarization [Figs. 3(e), 3(f)] secondary features develop greater relative intensity and the even and odd maps look quite different. As expected, the emission around $\bar{M}$ from the second sheet is suppressed in this polarization, making these maps unsuitable to address this aspect of the electronic structure. On the other hand, the trace of the FS sheets is reinforced along the lattice modulation direction via superposition with its Umklapp images, thereby distorting the image of the hole sheet in the odd map [Fig. 3(e)], indicating that caution must be exercised in deducing physical parameters (size and shape) from this spectrum. The mix of primary and secondary features is quite different in the 32 eV data, Fig. 4, even though some of the characteristics are basically similar. For example, the second FS sheet is emphasized in the even polarization in Figs. 4(a), 4(b), but suppressed in the odd case of Figs. 4(c), 4(d). Compared to 21.2

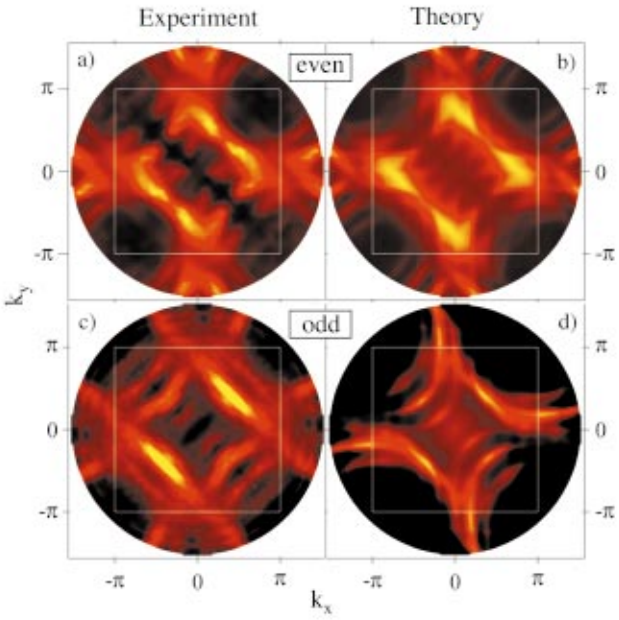

FIG. 4. (Color) Same as Fig. 3, except that this figure refers to 32 eV synchrotron light.

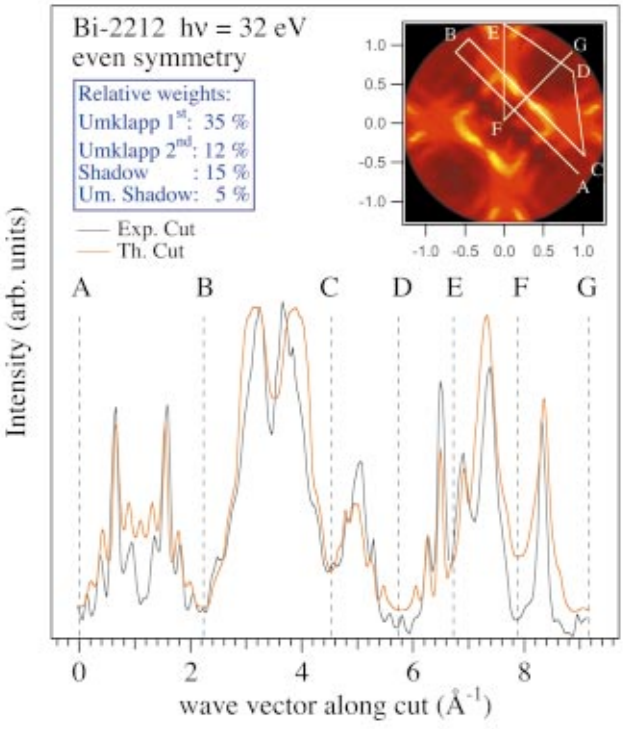

FIG. 5. (Color) Inset: Fermi surface map at 32 eV photon energy (even symmetry), showing the segmented line A-G along which ARPES intensity was considered for obtaining the weights of Table I. Main frame: Experimental ARPES intensity (thick line) along the line segments A-G in inset is compared with the corresponding theoretical fit (thin line) obtained by adding contributions of various modulations with appropriate weights as described in the text.

eV, there is generally a greater spectral weight at higher momenta; for example, the image of the second sheet is more or less equally intense in the first and second BZ's in Figs. 4(a), 4(b), but in the 21.2 eV Figs. 3(c), 3(d), the second BZ imprint is quite weak in relation to that in the first BZ. The combination of the two FS sheets with appropriately weighted secondary images yields two nearly parallel bands of intense emission which are oriented along the $(\pi,-\pi)$ direction in Fig. 4 and appear quite striking. Interestingly, in even polarization [Figs. 3(c), 3(d) or 4(a), 4(b)] the spectra show a remarkable line of essentially zero intensity along the $\bar{\Gamma}\rightarrow\bar{Y}$ direction, as expected for a mirror plane. However, along the perpendicular line $\bar{\Gamma}\rightarrow\bar{X}$, this is not true since the superlattice compromises the symmetry.

As noted in the Introduction, the determination of the FS topology of the underlying tetragonal phase in Bi2212 has been complicated by the presence of secondary features tied to superlattice and shadow bands. The results of Table I offer insight into how a headway can be made in disentangling primary and secondary features by exploiting the energy and polarization dependencies of the ARPES matrix element. We see that in the 21.2 eV even geometry, no secondary feature displays a weight greater than 20% of the primary features, and therefore, this energy and polarization is well suited for delineating the primary FS. In sharp contrast, the weights of secondary features are significantly greater at 32 eV in both the even and odd spectra as well as in the 21.2 eV odd spectrum. Interestingly, the shadow feature is most prominent in the 32 eV odd case, and the second superlattice image is visible in 32 eV even map, albeit weakly.

Although *absolute* intensities are not our focus, one aspect of these is particularly germane to this discussion. The theoretically computed[33] maximum absolute ARPES intensities of the *primary* features are in the ratios 21.2 eV (even): 21.2 eV (odd): 32 eV (even): 32 eV (odd) = 5:2:1.2:0.7, in reasonable accord with the corresponding experimental values of 5:1.7:0.8:0.6, uncertainty in determining absolute experimental intensity notwithstanding. Applying these ratios to the data of Table I (which gives the relative weights of the secondary features), it is found that the absolute intensities of various *secondary* features are not all that different at the two photon energies considered for either the odd or the even maps. In other words, the primary emissions become highlighted in the 21.2 eV even measurements not because the secondaries are weak, but due to the primaries becoming much stronger.

It has sometimes been suggested that the superlattice features do not reflect the dispersion of the CuO_2 planes, but arise from a diffraction effect when the photoelectron passes through the distorted BiO layer.[34] The present results indicate that this is not the case, but that a modulation exists within the CuO_2 planes. For a diffraction effect, one would expect the matrix element to govern the primary electron emission event, and therefore, expect the intensities of the secondary peaks to roughly scale with those of the primary peaks. This, however, is clearly not the case from Table I, where the relative weight of the secondary features is considerably larger for the 32 eV odd data than for the 21.2 eV even data. Along these lines, a close examination of Figs. 3 and 4 reveals that, in the odd maps of Figs. 3(e), 3(f) or 4(c), 4(d), the theoretical and experimental intensities of various features and the connectivity of bands in some cases do not quite match up. In this connection, some confirmatory evidence for the modulation of CuO_2 planes may be noted as follows. (1) The compound $Bi_{10}Sr_{15}Fe_{10}O_{46}$ is isostructural with Bi2212, except that it has a *commensurate* 5×1 superlattice with known local atomic displacements.[35] A considerable modulation of the Fe positions is found. We have incorporated these displacements into a tight-binding model of a hypothetical 5×1 modulated CuO_2 plane assuming the Cu positions to be the same as the observed Fe positions and using the known dependence of hopping parameter t on Cu-O distance.[36] We find superlattice modulation effects of the order of 10% of the primary features, which are comparable to the present observation.[37] (2) The superlattice modulations observed in photoemission spectra are considerably stronger in the single layer compound,[38] consistent with an enhanced modulation of the CuO_2 planes—a bilayer being less easily deformed than a single layer, but unexpected on a diffraction model since the BiO layer is identical in both cases. (3) Misra *et al.*[39] report direct tunneling into a CuO_2 plane which lacks a BiO overlayer. They report clear evidence for modulation of the CuO_2 planes on this basis. (4) It should finally be noted that the modulation of the CuO2 plane would induce an intrinsic Fermi surface anisotropy. If so, then Ando *et al.*[40] are not justified in ignoring this factor as a possible cause of the novel anisotropy they observed in the thermal conductivity of Bi2212 with respect to the superlattice modulation axis. A full description of the ARPES spectra of Bi2212 will eventually require a proper treatment of the effects of various modulations and the related 3D electronic structure.

V. CONCLUSIONS

In conclusion, we demonstrate that dramatic differences in the observed FS maps under various experimental conditions arise as a simple consequence of the ARPES matrix element which gives the primary FS features (arising from the underlying tetragonal lattice) a weight which depends upon the energy and polarization of light in a *very different manner* from that of the secondary features associated with the superlattice and orthorhombic modulations. In this way the ARPES matrix element helps disentangle various aspects of the electronic structure and fermiology of this complex system. In particular, we demonstrate that theory can help determine the number of primary FS sheets in Bi2212, confirming recent results.[2,3,5,7]

The wide ranging accord between theory and experiment indicates that the band theory framework implicit in the computations captures the essential underlying physics, suggesting that the two FS sheets in Bi2212 mainly reflect conventional bilayer splitting. However, it is likely that other effects (e.g., strong electron-phonon coupling and/or some form of nanoscale phase separation or stripe order) will need to be incorporated into the final picture. A detailed exploration of the growing role of strong correlations at lower doping and

temperatures, where bilayer splitting is expected to decrease while effects due to pseudogaps, stripes, and nanoscale phase separation become more prominent, should prove worthwhile.

ACKNOWLEDGMENTS

We acknowledge support by the Spanish agency MCYT under Grant No. MAT2002-03431. The authors also thank the W-31-109-ENG-38 and AC0298CH10886 contracts and the large scale Installation Program of the EU. We gratefully acknowledge the Northeastern University Advanced Scientific Computation Center (ASCC) for the allocation of supercomputer time at the NERSC.

APPENDIX: ESTIMATION OF WEIGHTS OF SECONDARY FEATURES

The procedure for determining weights of Table I is described here with reference to Fig. 5, which considers the 32 eV spectrum for even polarization as an example. First, the intensity from the experimental FS map is determined along a cut consisting of several straight segments in the (k_x, k_y) plane, chosen to intersect the maximal number of spectral features, including the main, shadow, and Umklapp bands. Along this cut, represented by line A-G in the inset to Fig. 5, the experimental and theoretical intensities are fitted. For this purpose the theoretical intensity of the secondary features throughout the (k_x, k_y) plane is determined by shifting the computed primary intensity for the tetragonal lattice by the corresponding translation vector $\eta(\pi,\pi)$ and assigning the associated weight (see Table I). The fitting process then only involves these weights as parameters. Figure 5 shows the high quality of the fit for the case of the Fermi surface map measured at 32 eV and even geometry detection. The weights in Table I have been obtained by carrying out such fits independently for the different indicated experimental conditions of photon energy and polarization.

*Electronic address: asensio@lure.u-psud.fr

[1] See, e.g., *Spectroscopies in Novel Superconductors*, edited by A. Bansil, R. Markiewicz, S. Sridhar, and D. Liebenberg [J. Phys. Chem. Solids **59**, (1998)], and other volumes in this series.

[2] D.L. Feng, N.P. Armitage, D.H. Lu, A. Damascelli, J.P. Hu, P. Bogdanov, A. Lanzara, F. Ronning, K.M. Shen, H. Eisaki, C. Kim, J.-i. Shimoyama, K. Kishio, and Z.-X. Shen, Phys. Rev. Lett. **86**, 5550 (2001).

[3] P.V. Bogdanov, A. Lanzara, X.J. Zhou, S.A. Kellar, D.L. Feng, E.D. Lu, H. Eisaki, J.-I. Shimoyama, K. Kishio, Z. Hussain, and Z.X. Shen, Phys. Rev. B **64**, 180505 (2001).

[4] Y.D. Chuang, A.D. Gromko, D.S. Dessau, Y. Aiura, Y. Yamaguchi, K. Oka, A.J. Arko, J. Joyce, H. Eisaki, S.I. Uchida, K. Nakamura, and Yoichi Ando, Phys. Rev. Lett. **83**, 3717 (1999).

[5] Y.-D. Chuang, A.D. Gromko, A. Fedorov, Y. Aiura, K. Oka, Yoichi Ando, H. Eisaki, S.I. Uchida, and D.S. Dessau, Phys. Rev. Lett. **87**, 117002 (2001).

[6] H.M. Fretwell, A. Kaminski, J. Mesot, J.C. Campuzano, M.R. Norman, M. Randeria, T. Sato, R. Gatt, T. Takahashi, and K. Kadowaki, Phys. Rev. Lett. **84**, 4449 (2000).

[7] A.A. Kordyuk, S.V. Borisenko, M.S. Golden, S. Legner, K.A. Nenkov, M. Knupfer, J. Fink, H. Berger, L. Forro, and R. Follath, Phys. Rev. B **66**, 014502 (2002).

[8] S.V. Borisenko, M.S. Golden, S. Legner, T. Pichler, C. Dürr, M. Knupfer, J. Fink, G. Yang, S. Abell, and H. Berger, Phys. Rev. Lett. **84**, 4453 (2000); A.A. Kordyuk, S.V. Borisenko, T.K. Kim, K.A. Nenkov, M. Knupfer, J. Fink, M.S. Golden, H. Berger, and R. Follath, *ibid.* **89**, 077003 (2002); A.A. Kordyuk, S.V. Borisenko, M.S. Golden, S. Legner, K.A. Nenkov, M. Knupfer, J. Fink, H. Berger, L. Forro, and R. Follath, Phys. Rev. B **66**, 014502 (2002).

[9] T. Sato, T. Kamiyama, Y. Naitoh, T. Takahashi, I. Chong, T. Terashima, and M. Takano, Phys. Rev. B **63**, 132502 (2001).

[10] We do not address the specific origin of the orthorhombic features which could arise from various mechanisms, e.g., orthorhombic lattice distortions, antiferromagnetic fluctuations, etc.

[11] P. Aebi, J. Osterwalder, P. Schwaller, L. Schlapbach, M. Shimoda, T. Mochiku, and K. Kadowaki, Phys. Rev. Lett. **72**, 2757 (1994).

[12] H. Ding, A.F. Bellman, J.C. Campuzano, M. Randeria, M.R. Norman, T. Yokoya, T. Takahashi, H. Katayama-Yoshida, T. Mochiku, K. Kadowaki, G. Jennings, and G.P. Brivio, Phys. Rev. Lett. **76**, 1533 (1996).

[13] N. Saini, J. Avila, A. Bianconi, A. Lanzara, M.C. Asensio, S. Tajima, G.D. Gu, and N. Koshizuka, Phys. Rev. Lett. **79**, 3467 (1997).

[14] X.J. Zhou, P. Bogdanov, S.A. Kellar, T. Noda, H. Eisaki, S. Uchida, Z. Hussain, and Z.-X. Shen, Science **286**, 268 (1999).

[15] T. Valla, A.V. Fedorov, P.D. Johnson, Q. Li, G.D. Gu, and N. Koshizuka, Phys. Rev. Lett. **85**, 828 (2000).

[16] J. Avila, C. Casado, M.C. Asensio, J.L Perez, M.C. Munoz, and F. Soria, J. Vac. Sci. Technol. A **13**, 1501 (1995).

[17] A. Mascaraque, J. Avila, E.G. Michel, and M.C. Asensio, Phys. Rev. B **57**, 14 758 (1998).

[18] J. Avila, A. Mascaraque, E.G. Michel, M.C. Asensio, G. LeLay, J. Ortega, R. Perez, and F. Flores, Phys. Rev. Lett. **82**, 442 (1999).

[19] S. Gallego, J. Avila, M. Martin, X. Blase, A. Taleb, P. Dumas, and M.C. Asensio, Phys. Rev. B **61**, 12 628 (2000).

[20] H. Ascolani, J. Avila, N. Franco, and M.C. Asensio, Phys. Rev. Lett. **78**, 2604 (1997).

[21] H. Ascolani, J. Avila, N. Franco, and M.C. Asensio, Phys. Rev. B **58**, 13 811 (1998).

[22] Y. Huttel *et al.*, Phys. Rev. B **61**, 4948 (2000).

[23] A. Bansil and M. Lindroos, Phys. Rev. Lett. **83**, 5154 (1999).

[24] A. Bansil and M. Lindroos, J. Phys. Chem. Solids **56**, 1855 (1995).

[25] M. Lindroos and A. Bansil, Phys. Rev. Lett. **75**, 1182 (1995).

[26] M. Lindroos and A. Bansil, Phys. Rev. Lett. **77**, 2985 (1996).

[27] A. Bansil and M. Lindroos, J. Phys. Chem. Solids **59**, 1879 (1998).

[28] K. Gofron, J.C. Campuzano, A.A. Abrikosov, M. Lindroos, A. Bansil, H. Ding, D. Koelling, and B. Dabrowski, Phys. Rev. Lett. **73**, 3302 (1994).

[29] A. Bansil and S. Kaprzyk, Phys. Rev. B **43**, 10 335 (1991).

[30] S. Kaprzyk and A. Bansil, Phys. Rev. B **42**, 7358 (1990).

[31] A. Bansil, S. Kaprzyk, P.E. Mijnarends, and J. Tobola, Phys. Rev. B **60**, 13 396 (1999).

[32] S. Massida, J. Yu, and A.J. Freeman, Physica C **152**, 251 (1988); H. Krakauer and W.E. Pickett, Phys. Rev. Lett. **60**, 1665 (1988); M.S. Hybertsen and L.F. Mattheiss, *ibid.* **60**, 1661 (1988).
[33] M. Lindroos, S. Sahrakorpi, and A. Bansil, Phys. Rev. B **65**, 054514 (2002).
[34] M.R. Norman, M. Randeria, H. Ding, and J.C. Campuzano, Phys. Rev. B **52**, 615 (1995).
[35] Y. Le Page, W.R. McKinnon, J.M. Tarascon, and P. Barboux, Phys. Rev. B **40**, 6810 (1989).
[36] R.S. Markiewicz (unpublished).
[37] There is an additional screening effect which should enhance the observed superlattice modulation: excess oxygen in the BiO layers provides a periodic Coulomb potential at the CuO_2 planes, which should lead to an additional modulation of the hole density. This effect is not included in the tight-binding calculation of Ref. 36.
[38] A. Lanzara and Z.-X. Shen (private communication).
[39] S. Misra, S. Oh, D.J. Hornbaker, T. DiLuccio, J.N. Eckstein, and A. Yazdani, Phys. Rev. Lett. **89**, 087002 (2002).
[40] Y. Ando, J. Takeya, Y. Abe, X.F. Sun, and A.N. Lavrov, Phys. Rev. Lett. **88**, 147004 (2002).